HIGH FIDELITY SIMULATIONS IN SUPPORT TO ASSESS AND IMPROVE RANS FOR MODELING TURBULENT HEAT TRANSFER IN LIQUID METALS: THE CASE OF FORCED CONVECTION

Yann Bartosiewicz[1]
[1]UCLouvain, Institute of Mechanics, Materials, and Civil Engineering, Place du Levant 2, 1348 Louvain la Neuve, Belgium, yann.bartosiewicz@uclouvain.be

ABSTRACT

This paper attempts to give a brief overview of the work conducted through some recent EU funded projects (THINS, SESAME and MYRTE) concerning the use of high fidelity simulations, namely Direct Numerical Simulations (DNS) and Large Eddy Simulations (LES), to adapt Reynolds Averaged Navier-Stokes (RANS) models for the computation of turbulent heat transfer in liquid metal conditions. The focus is made on forced convection only, that prevails in normal reactor operation, and through some selected cases performed at UCLouvain, e.g. the channel flow and the impinging jet. The considered RANS approaches are the models based on the simple Reynolds analogy (simple gradient diffusion hypothesis or SGDH) and the algebraic heat flux variants (implicit and explicit).

KEYWORDS
Liquid metal, low Prandtl number heat transfer, high fidelity simulations (LES and DNS)

1. INTRODUCTION

Liquid Metal Reactors (LMR) are characterized, from the thermal-hydraulic point of view, by a very low Prandtl number coolant, $Pr = \nu/\alpha \approx 0.01$, with ν the kinematic viscosity and α the heat diffusivity. At such Prandtl number, the temperature field is much smoother than the velocity field, i.e. the smallest temperature scales are much larger than those of the velocity, and, even for high Reynolds numbers, the heat transfer could be essentially molecular while the flow is fully turbulent. Consequently, simulation tools and in particular Computational Fluid Dynamics (CFD) should account for such peculiar behavior. We can classify CFD by three distinct approaches according the level of modeling/simulating the flow physics: the Direct Numerical Simulation (DNS), the Large Eddy Simulation (LES), and the Reynolds Averaged Numerical Simulation (RANS). The flow physics of interest is essentially characterized by turbulent transfers, e.g. momentum and energy transfers. Turbulent flows are characterized by a full spectrum of space and time scales, ranging from large scales, driven by the geometry and boundary conditions, down to the smallest scales where the energy is finally dissipated. This feature is illustrated by the so-called energy cascade introduced by [1] and depicted by Figure 1 showing the turbulent kinetic energy $E(k)$ contained by eddies of size $1/k$, k being the local wave number. Basically, the energy is injected at scales related to the geometry and boundary conditions, and this energy cascades from the large scales of the flow and dissipates at smallest scales, also called the Kolmogorov scale η, according to a law scaling as $k^{-5/3}$ [1] (Figure 1). Hence the dissipation rate of the turbulent kinetic energy ϵ is set along the inertial range of the cascade, as under equilibrium conditions, the transfer rate between scales equals the dissipation rate. In this paper, the vocabulary high fidelity (HiFi) simulations refers to DNS and LES. It is considered that such simulations are able to accurately capture the above mentioned peculiar behavior of heat transfer in low Prandtl fluids. Indeed, as shown in Figure 1, DNS are supposed to resolve the full spectrum of wave numbers down to the Kolmogorov scale k_η, imposing a strong constraint on the mesh resolution $h_{DNS} \leq 2\eta$. LES explicitly solves the full physics as DNS but along a truncated spectrum. The truncation is generally explicitly imposed by the grid [2, 3] at a cutoff wave number $k_c = \pi/h_{LES}$. A challenging LES requires $h \gtrsim 30\eta$ which is roughly the transition between the inertial range and the dissipation range.

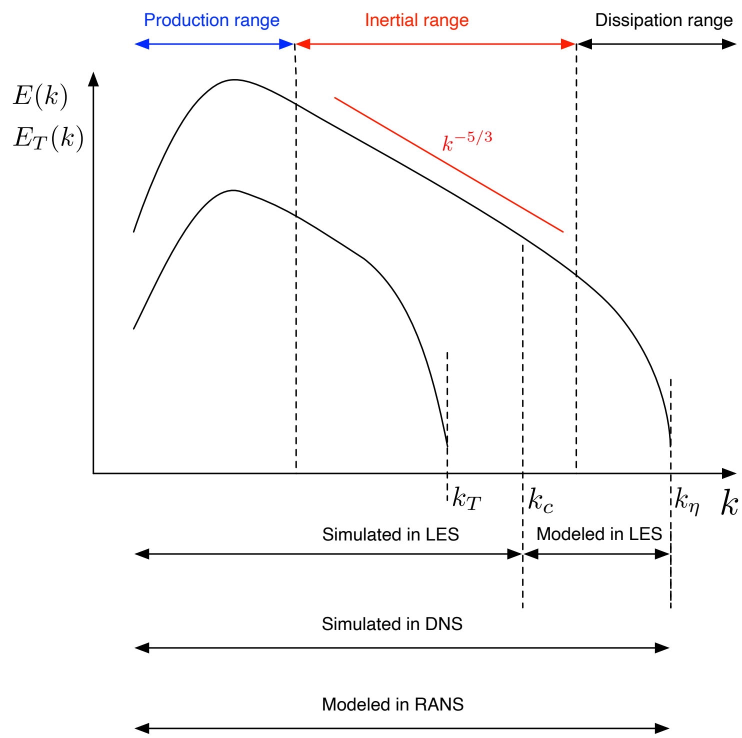

Figure 1. Kinetic energy (E) and temperature variance(E_T) spectra for Liquid metals.

As for the spatial scales, we can introduce the scalar diffusion cutoff length also called the Obukhov-Corrsin [4] scale η_T which is related to the Kolmogorov scale by

$$\eta_T = \left(\frac{\alpha^3}{\epsilon}\right)^{1/4} = \left(\frac{1}{Pr}\right)^{3/4} \eta_K. \tag{1}$$

Hence it is possible to relate the cutoff wavenumber for the temperature to the Kolmogorov cutoff:

$$k_T = Pr^{3/4} k_\eta, \tag{2}$$

which shows that $k_T \approx 0.03 k_\eta$ for liquid metals ($Pr \approx 0.01$). Such a temperature spectrum is overlapped on the Figure 1 and illustrates an interesting feature. Indeed because in the offset of both spectra, there is a range of cutoff wavenumbers to achieve a LES for the velocity field while resolving the smallest scales of the temperature field. In other words, it is possible to achieve a hybrid simulation which is a LES for the velocity and a DNS for the temperature (further noted in this paper as V-LES/T-DNS). In [5], the author indicates the grid requirement for achieving a DNS of a temperature field, e.g. $h/\eta_T < 1$ for close to unity Prandtl number fluids, could give $h/\eta_T < 3.45$ for a liquid metal. This condition could be used *a posteriori* to check that the LES was indeed a T-DNS. In this respect, as far as challenging LES are performed under the previous mentioned criterion, they can be considered as reference data (as DNS) for the turbulent heat transfer in liquid metals as a support to improve the RANS approach. Indeed as pointed out by [6], measuring high resolution local data in liquid metal conditions, as required for CFD grade experiments, is very challenging. Although high quality experiments become available [7, 8], high fidelity simulations represent a trustworthy source of diverse data for calibration and assessment of existing as well as newly RANS techniques [7, 9] in the case of liquid metal heat transfer.

Contrary to HiFi simulations, RANS does not explicitly solve the physics but on the contrary requires turbulence models along the full space-time spectrum to mimic the correct physics. Basically, such turbulence heat flux models mainly rely on a structural coupling between the velocity and the temperature fields, also known as the so-called Reynolds analogy [10]. As a result, the eddy diffusivity concept was naturally introduced and linked to the eddy viscosity concept by a turbulent Prandtl number (Pr_t), this approach is the so-called simple gradient diffusion hypothesis (SGDH) as explained in [11, 12]. It is well known that this concept, initially calibrated for fluids with $Pr \approx \mathcal{O}(1)$, fails for liquid metals [13], as well as for some buoyant flows when the temperature variance and the ratio of the thermal to mechanical scales are important [14, 15]. This is the reason why the modeler community has been performing extensive researches during the last decades to not only improve the existing Reynolds analogy approach and define new best practice guidelines (BPG) [16, 17], but also to define new approaches such as implicit [18, 19] or explicit (4-equation model, known as $k - \epsilon - k_\theta - \epsilon_\theta$) [20, 21] Algebraic Heat Flux Models (AHFM).

The objective of this paper is to give an overview of high fidelity simulations of forced convection heat transfer at low Prandtl performed at UCLouvain and how those simulations were used to (i) improve the classical Reynolds analogy for industrial calculations of wall-bounded liquid metal flows, and to (ii) qualify the above mentioned advanced AHFM-RANS models.

For more general results concerning other flow regimes such as mixed or natural convection and other test cases, the reader should refer to [7, 12, 22].

2. HOW HIFI SIMULATIONS IMPROVED RANS IN FORCED CONVECTION: SELECTED CASES

2.1. Flow solver

The governing equations are discretized in space using the fourth order finite difference scheme of [23], which is such that the discretized convective term conserves the discrete energy on cartesian stretched meshes. This is an important characteristic for HiFi numerical simulations of turbulent flows. The Poisson equation for the pressure is solved using an efficient parallel multigrid solver which is either used directly or as a preconditioner for a conjugate gradient solver. The equations are integrated in time using a second order Adams-Bashforth time-stepping. At low Prandtl number, subtime-stepping is used for the temperature equation because of the very small heat conduction time-scale which is more stringent that the convective time-scale, i.e. the CFL condition. For LES, the sub-grid scale is a multiscale version of the so-called WALE model [24]. This implementation is performed in an in-house code at UCLouvain called BigFlow. Full details about LES in liquid metals using this approach can be found in [2, 3].

2.2. Channel flows

The periodic channel flow configuration (Figure 2) is a generic case for RANS assessment of developed wall-bounded flows. This type of flow is interesting to investigate both the value of the turbulent Prandtl number in the bulk but also the near-wall heat transfer and hence the near wall modeling strategy for RANS (wall-function-RANS). At the reactor scale, this obviously applies for the flow along fuel pins as well as in any heat exchanger under normal conditions (forced convection). This case is numerically tackled by

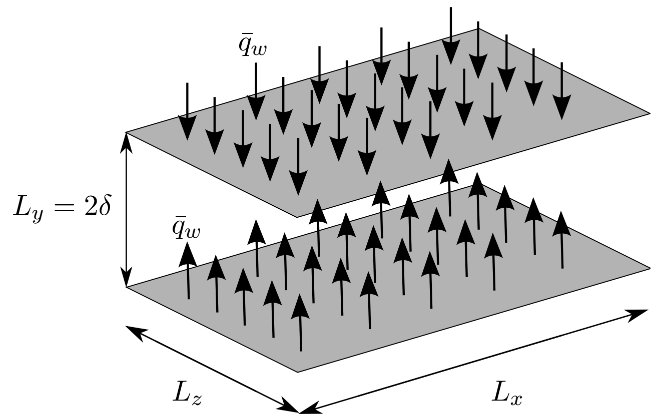

Figure 2. Channel flow configuration. The arrows symbolize the wall heat flux.

computing a time-developing flow between two plates with periodic boundary conditions in the streamwise (x) and spanwise (z) directions. The flow is characterized by the Reynolds number based on the friction velocity $\bar{u}_\tau$: $Re_\tau = \frac{\bar{u}_\tau \delta}{\nu}$ where $\bar{u}_\tau$ is related to the wall shear stress: $\bar{u}_\tau^2 = \bar{\tau}_w/\rho$, δ is half the channel width and ν is the kinematic viscosity. Furthermore, it is important to mention that the thermal boundary condition is equivalent to imposing an averaged heat flux (not the total heat flux) or a linear temperature variation along the streamwise direction; this is achieved for a periodic flow by solving the energy equation for a modified temperature θ, and imposing $\theta = 0$ at walls [2]. Table I summarizes the different high-fidelity simulations performed at UCLouvain for this case with their corresponding reference DNS. Although a large range of Reynolds and Prandtl numbers was covered, the focus will be made here on selected results at low Prandtl number. As mentioned in the introduction, at low Prandtl numbers ($Pr \approx \mathcal{O}(\,0.01\,)$), one can take advantage of performing hybrid simulations, e.g. LES for the momentum field and DNS for the temperature field, also called V-LES/T-DNS. It worth mentioning here that all LES performed were challenging LES as described in the introduction and all were wall-resolved LES with a subgrid scale showing a correct asymptotic behavior. The reader is invited to check the related references for more information on the mesh resolution in each direction. Figure 3 illustrates this V-LES/T-DNS characteristics for $Re_\tau = 590$ and $Pr = 0.01$. It is clear that the LES grid fully resolves the temperature field which depicts much larger scale structures than the velocity field. The validity of this approach is confirmed by looking at the comparison with the DNS results (Figure 3 bottom), where both the mean temperature and its RMS are very well predicted by the LES. Another remarkable features on the mean temperature profile, are (i) the absence of any log-behavior as it is the case for the velocity profile (not shown here but in [16]), and (ii) the unusual extension of the linear law up to $y^+ \approx 60$ which corresponds to the very lower bound of the log-profile for the velocity [16, 17]. This shows the difficulty to use a direct mapping with the momentum transfer near walls by using the usual wall-function for the temperature as it is the case for RANS approach based on the full- or partial-Reynolds analogy (e.g. models based on a SGDH assumption and a Pr_t). Furthermore such simple models usually require a turbulent Prandtl number Pr_t not only for the wall-function, but also for the evaluation of the turbulent heat diffusivity in the bulk. For this point HiFi, simulations are of great value as it is possible to reconstruct the turbulent Prandtl number from high resolution results:

$$Pr_t = \frac{\nu_t}{\alpha_t} = \frac{\overline{u'v'}}{\overline{v'\theta'}} \frac{\frac{d\bar{\theta}}{dy}}{\frac{d\bar{u}}{dy}}. \tag{3}$$

Table I. Parameters used for the channel flow simulations at UCLouvain and the reference DNS

		Re_τ	$Re_{2\delta}$	Pr	$L_x \times L_y \times L_z$	$n_x \times n_y \times n_z$
Kawamura [25]	DNS	180	5600	$0.025 \dots 1$	$6.4\delta \times 2\delta \times 3.2\delta$	$128 \times 128 \times 128$
UCLouvain [16]	DNS	180	5600	$0.01 - 0.1 - 1$	$2\pi\delta \times 2\delta \times \pi\delta$	$128 \times 128 \times 128$
Tiselj [26]	DNS	590	22 000	0.01	$2\pi\delta \times 2\delta \times \pi\delta$	$384 \times 257 \times 384$
UCLouvain	DNS	590	22 000	$0.01 - 0.025$	$5.75\delta \times 2\delta \times 2.9\delta$	$384 \times 384 \times 384$
UCLouvain [16]	LES	590	22 000	$0.01 - 0.025$	$2\pi\delta \times 2\delta \times \pi\delta$	$96 \times 64 \times 96$
Kawamura [27]	DNS	640	24 400	0.025	$12.8\delta \times 2\delta \times 6.4\delta$	$1024 \times 256 \times 1024$
UCLouvain [28]	LES	640	24 400	$0.01 - 0.025$	$2\pi\delta \times 2\delta \times \pi\delta$	$96 \times 64 \times 96$
Jimenez [29]	DNS	2000	87 000		$8\pi\delta \times 2\delta \times 3\pi\delta$	$6144 \times 633 \times 4608$
UCLouvain [17]	*LES*	2000	87 000	$0.01 - 0.025$	$2\pi\delta \times 2\delta \times \pi\delta$	$384 \times 256 \times 384$

Figure 4 illustrates the results obtained by the performed HiFi simulations for Pr_t at different Reynolds numbers and for $Pr = 0.01$ (left and right) or $Pr = 0.025$ (right). It is interesting to note (Figure 4 left) that all the curves collapse, except for $Re_\tau = 180$ which is too low to be representative of a fully turbulent flow. The turbulent Prandtl number shows a peak close to the wall and decreases to reach a plateau-like behavior in the bulk. This demonstrates the inadequacy of using a single value of $Pr_t \approx 0.85$ as in RANS based on the Reynolds analogy. However, attempting to find a relation $Pr_t = f(y^+, Pr)$ from the wall to the bulk would be also useless since very close to the wall only molecular effects yet hold (α_t should tend to zero [17]) and are even dominating up to $y^+ \approx 60$ as previously observed (Figure 3 left). As demonstrated in details in [17], among the tested correlation for Pr_t, that of Kays [30],

$$Pr_t = 0.85 + \frac{0.7}{Pe_t}, \tag{4}$$

is the one which provides the best results for the tested Reynolds and Prandtl numbers. Figure 4 (right) shows that this local correlation well envelops the obtained Pr_t by the different HiFi simulations. The plateau value is generally well predicted by the correlation as well as the singular near wall behavior, which should not be an issue in codes since it will provide a turbulent heat diffusivity tending to zero.

Such HiFi simulations were also helpful to define a new temperature wall-function suited for low Prandtl numbers. By Integrating the heat flux balance equation, keep both the molecular and the turbulent component, [17] developed a mixed-wall-function:

$$\bar{\theta}^+ = \frac{Pr_t}{\kappa} \log\left(1 + \frac{\kappa}{Pr_t} Pr\, y^+\right), \tag{5}$$

where a value of $Pr_t = 2$ provided the best overall fit and agreed well with the observations (Figure 4). This equation relies on the assumption of a linear model of the turbulent heat diffusivity outside of its y^{+3}

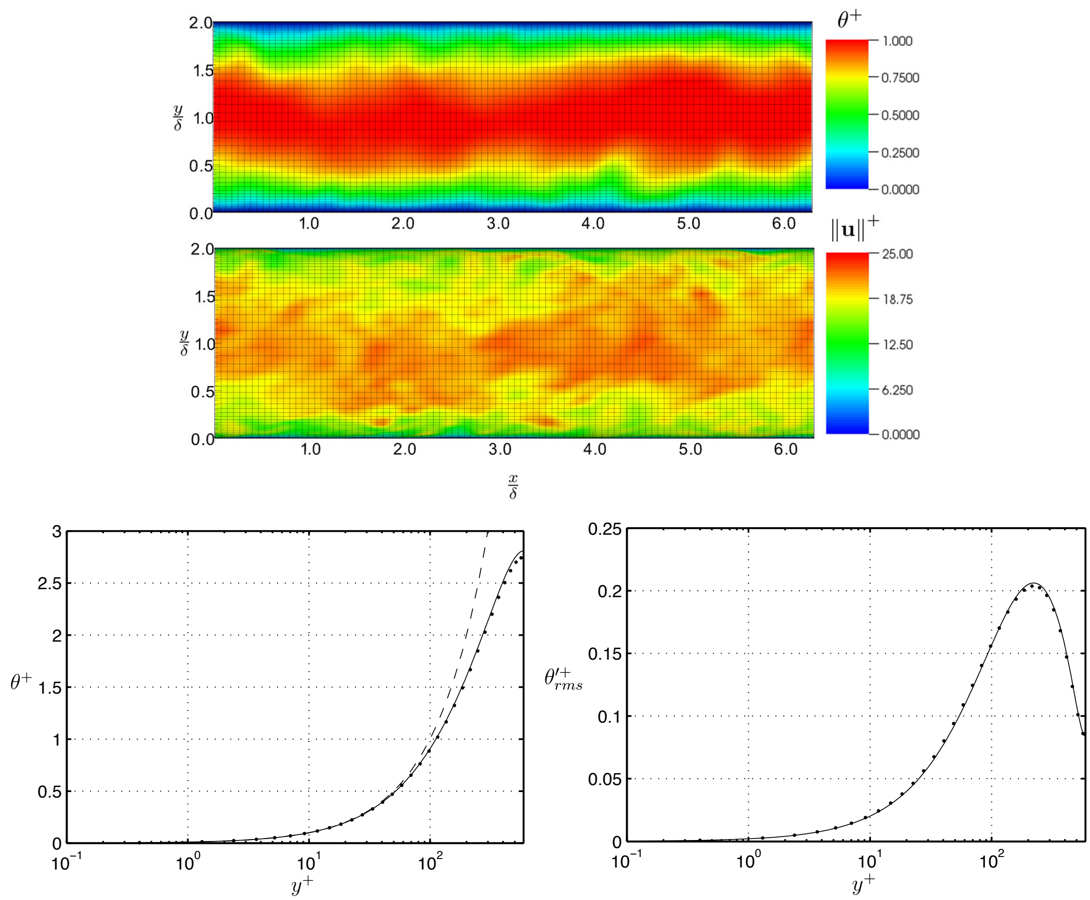

Figure 3. $\boldsymbol{Re_\tau = 590}$ **and** $\boldsymbol{Pr = 0.01}$**. Plane cut in the temperature field and in the velocity magnitude field at a given time (top). The LES grid is superimposed. Mean temperature(bottom left) and its RMS (bottom right) profiles. Present work LES(bullets), DNS (solid), theoretical near wall behaviour** $\boldsymbol{\theta^+ = Pr\, y^+}$ **(dash).**

behavior very close to the wall [17]. This wall-function showed its better performance for low-Prandtl [17] than the well-known existing blending approach of Kader [31], which extends the linear law too far away from the wall and the blending does not yield an accurate profile in the near-wall region, for $1 \leq Pr\, y^+ \leq 6$, where the first grid point would be typically placed when using wall-functions. Figure 5 (left) displays this mixed-wall-function versus the mean temperature profiles obtained by HiFi simulations at different Re_τ and $Pr = 0.01 - 0.025$. This new wall-function provides very good agreement up to $Pry^+ \approx 3$ which corresponds to $y^+ \approx 300$. The proposed new BPG for RANS based on the SGDH and Reynolds analogy is then to use the Kays correlation for Pr_t and the new mixed-wall-function. This was assessed in [17] and depicted in Figure 5 (right). This plot clearly shows that using the Kays correlation significantly improves the prediction of the mean temperature profile. Furthermore, using a wall-function RANS with the mixed-wall-function and a first grid point at $y^+ = 200$ provides as good results as the same model using a wall-resolved approach with a first grid point at $y^+ \approx 1$.

As mentioned in the introduction, over the last years, more advanced RANS models were developed for simulations of liquid metals. They are essentially based either on an implicit algebraic heat flux model such as the AHFM-NRG [18, 19] , or on an explicit variant as the $k - \epsilon - k_\theta - \epsilon_\theta$ [20, 21], both being basically

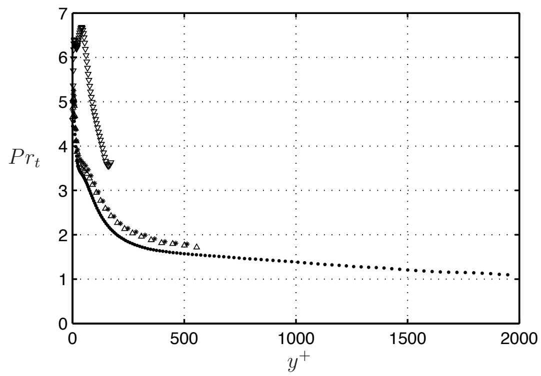

Figure 4. Turbulent Prandlt number. Left: $Pr = 0.01$, DNS at $Re_\tau = 180$ ($\bigtriangledown$), LES at $Re_\tau = 590$ ($*$), LES at $Re_\tau = 640$ ($\triangle$), LES at $Re_\tau = 2000$ ($\cdot$). Right: Turbulent Prandtl number as a function of $Pe_t = \frac{\nu_t}{\nu} Pr$: correlation of Kays [30] (solid line). Simulations at $Pr = 0.01$, i.e. DNS at $Re_\tau = 180$ ($\bigtriangledown$), LES at $Re_\tau = 590$ ($*$), LES at $Re_\tau = 640$ ($\triangle$) and LES at $Re_\tau = 2000$ ($\cdot$) and simulations at $Pr = 0.025$, i.e. LES at $Re_\tau = 590$ ($\square$), LES at $Re_\tau = 640$ ($\diamond$) and LES at $Re_\tau = 2000$ ($\circ$).

wall-resolved models. The main difference between both approach is that the AFM-NRG model does not use the SGDH and then takes into account the non-isotropy of the heat flux, while the $k - \epsilon - k_\theta - \epsilon_\theta$ is based on the isotropic approach of the SGDH. The AFM-NRG model has been calibrated on a wide range of operating conditions from the natural convection to the forced convection. Particularly in forced convection, the value of the constant C_{t1} (related the thermal production term of the turbulent heat flux algebraic equation) has been found to play a key role and a correlation has been developed on multiple channel flow HiFi simulations [18], $C_{t1} = 0.053ln(RePr) - 0.27$ with $Pe = RePr > 180$. Figure 6 shows a selected result for the case $Re_\tau = 590$ and $Pr = 0.01$ [16]. The AHFM-NRG clearly gives better

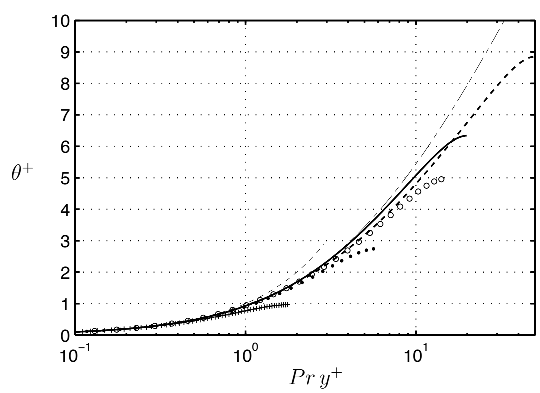

Figure 5. Mean temperature profiles. Left: DNS at $Re_\tau = 180$ and $Pr = 0.01$ ($+$), LES at $Re_\tau = 590$ and $Pr = 0.01$ ($\cdot$), LES at $Re_\tau = 590$ and $Pr = 0.025$ ($\circ$), LES at $Re_\tau = 2000$ and $Pr = 0.01$ (solid) and LES at $Re_\tau = 2000$ and $Pr = 0.025$ (dash). The linear law, $\bar{\theta}^+ = Pr\, y^+$, is plotted (thin dash) as well as the mixed law Eq. (5) (thin dash-dot). Right:$Re_\tau = 2000$ and $Pr = 0.01$, linear-law and $Pr_t = 0.85$ (thin solid and $\diamond$), mixed-law-wall function with $y_1^+ = 200$ and correlation of Kays (thin solid and $\circ$), LES (thick solid), wall-resolved RANS using the correlation of Kays (thin dash), theoretical linear law, $\bar{\theta}^+ = Pr\, y^+$ (thick dash-dot).

performances for both the mean temperature as well as its RMS compared to the other versions and to a wall-resolved $k-\epsilon$ model using the partial Reynolds analogy with $Pr_t = 0.9$. It was expected since the AHFM-cc is the calibrated version of the original AHFM-2005 [18] for forced convection and $Pr \approx 1$. Figure 7 illustrates the same type of results for the other approach, e.g. the $k-\epsilon-k_\theta-\epsilon_\theta$ of [20]. In this case the model overpredicts the LES mean temperature at $Re_\tau = 2000$ and $Pr = 0.025$ for $y^+ > 100$. This model was calibrated on the channel flow cases of Kawamura [27] up to $Re_\tau = 640$; in this case, the momentum model, more important at this Peclet number and for $y^+ > 100$ does not give more accurate results for the mean velocity profiles (see [32] to see more results concerning this case). However the results are significantly improved compared to the basic approach based on the usual Reynolds analogy [32].

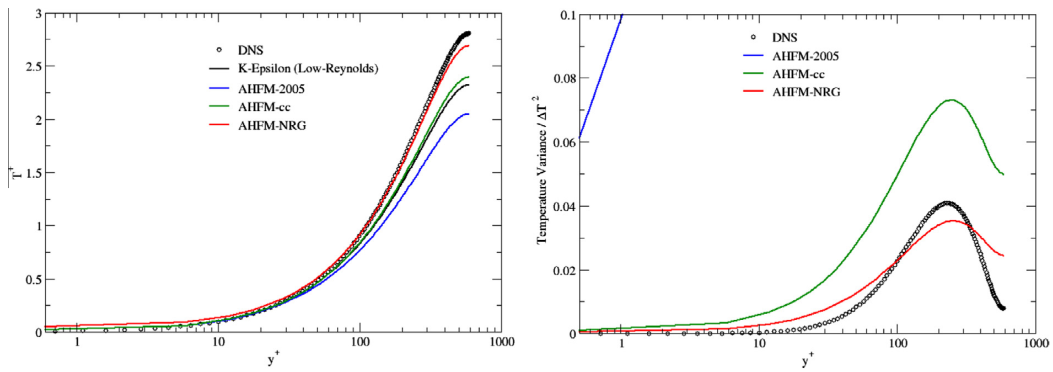

Figure 6. Comparison of the AHFM-NRG model and DNS results [16]in the case of $Re_\tau = 590$ and $Pr = 0.01$, taken from [18].

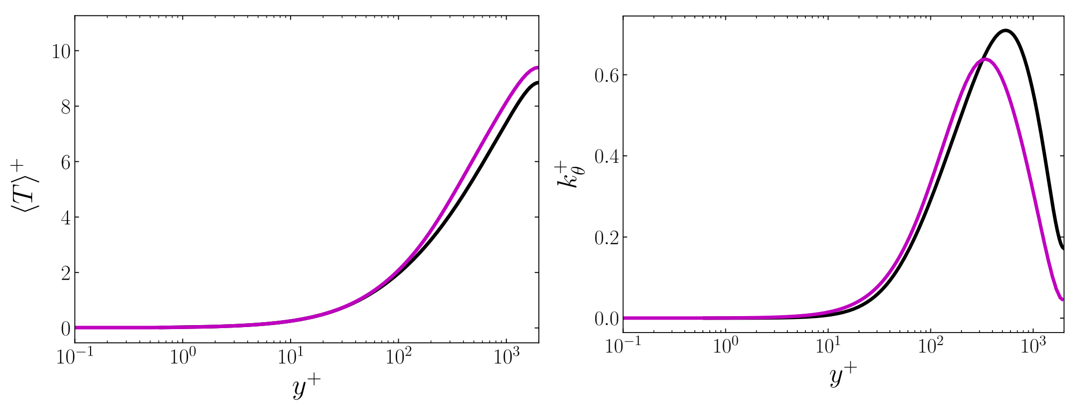

Figure 7. $Re_\tau = 2000$ and $Pr = 0.025$. Left: mean temperature profile. Right: $k_\theta{}^+ = \left(\theta'^+_{rms}\right)^2/2$. DNS (black), $k-\epsilon-k_\theta-\epsilon_\theta$ (magenta). Taken from [32].

2.3. Impinging jet

The impinging jet constitutes a challenging case of bounded but developing flow contrary to the channel where the flow was fully developed. The setup of the plane impinging jet consists of two infinite parallel flat plates where the top plate is split by a slit through which fluid is injected to form the jet, which impinges on the bottom plate. The problem is simulated in a rectangular box where the top ($y = H$) and bottom ($y = 0$) surfaces coincide with the walls and the top surface also contains the slit ($y = H$ and $-B/2 <$

Table II. Simulation parameters

	Re_B	Pr	$L/B \times H/B \times W/B$	$N_x \times N_y \times N_z$	Inlet
L4000	4000	1.0-0.1-0.01	$80 \times 2 \times \pi$	$2048 \times 144 \times 128$	flat laminar
T4000	4000	1.0-0.1-0.01	$80 \times 2 \times \pi$	$2048 \times 144 \times 128$	fully turbulent
T5700	5700	1.0-0.1-0.01	$80 \times 2 \times \pi$	$2560 \times 192 \times 128$	fully turbulent

$x < B/2$). In the mean flow direction, far away from the jet, at $x = -L/2$ and $L/2$, convective outflow boundary conditions are used, whereas the flow is considered periodic in the spanwise direction (z), in which the domain length is W. This configuration is sketched in Figure 8 (left). The top and bottom walls are isothermal, so that $u_i = 0$ and $T = T_w$ when $y = 0$ and when $y = H$ and $|x| \geq B/2$. In the slit ($y = H$ and $|x| < B/2$), the inlet jet profile is imposed. Two cases were considered: (i) a laminar inlet where a flat velocity was imposed, (ii) a turbulent inlet where a channel co-simulation was feeding a turbulent inlet velocity profile. The different cases are presented Table II. As the interest of this paper is to show how HiFi simulations contributed to improve/assess RANS in the case of liquid metal, and because RANS models are not suited to capture the physics of transitional flows, the selected case of interest is the T4000. In this case, the co-simulation channel is a case at $Re_\tau = 133$, which is even lower than the smallest Reynolds number ($Re_\tau = 180$) tested for the channel simulations. More details concerning the simulation parameters and results could be found in [33].

The main flow features of the T4000 case are depicted Figure 8 (right). The velocity magnitude, the spanwise vorticity ω_z and the temperature fields at $Pr = 1$ and $Pr = 0.01$ are displayed. The turbulent fluctuations in the jet are well visible at the inlet in vorticity fields. This results in an enhanced mixing of the jet which is already well-mixed after the impingement, at around $x/B = 3$. Consequently, for the temperature at $Pr = 1$, the isothermal core at T_j does not penetrate as far as in the L4000 case (not shown), as it mixes faster. At lower Pr, the differences are less pronounced because of the smoothing effect by the higher molecular diffusivity. Here the decoupling with the momentum field as the Prandtl number is decreased is obvious. Figure 9 shows the streamwise friction coefficient of the bottom wall, and Nusselt numbers. Elongated

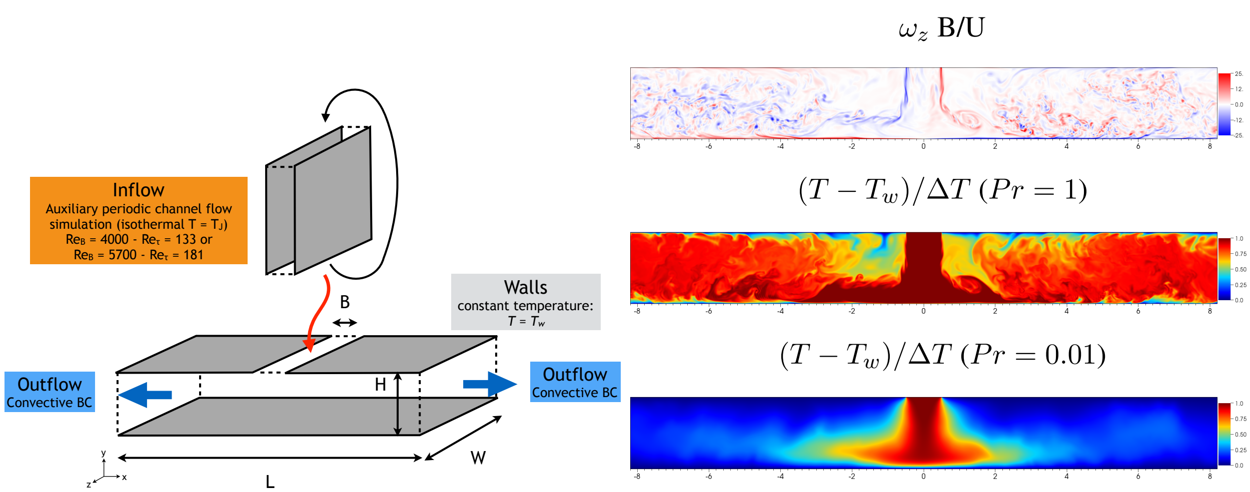

Figure 8. Computational setup (left). Visualizations of the instantaneous flow field in an arbitrary $x - y$ plane for the T4000 Case. Only the region $|x|/B < 8$ is shown (right).

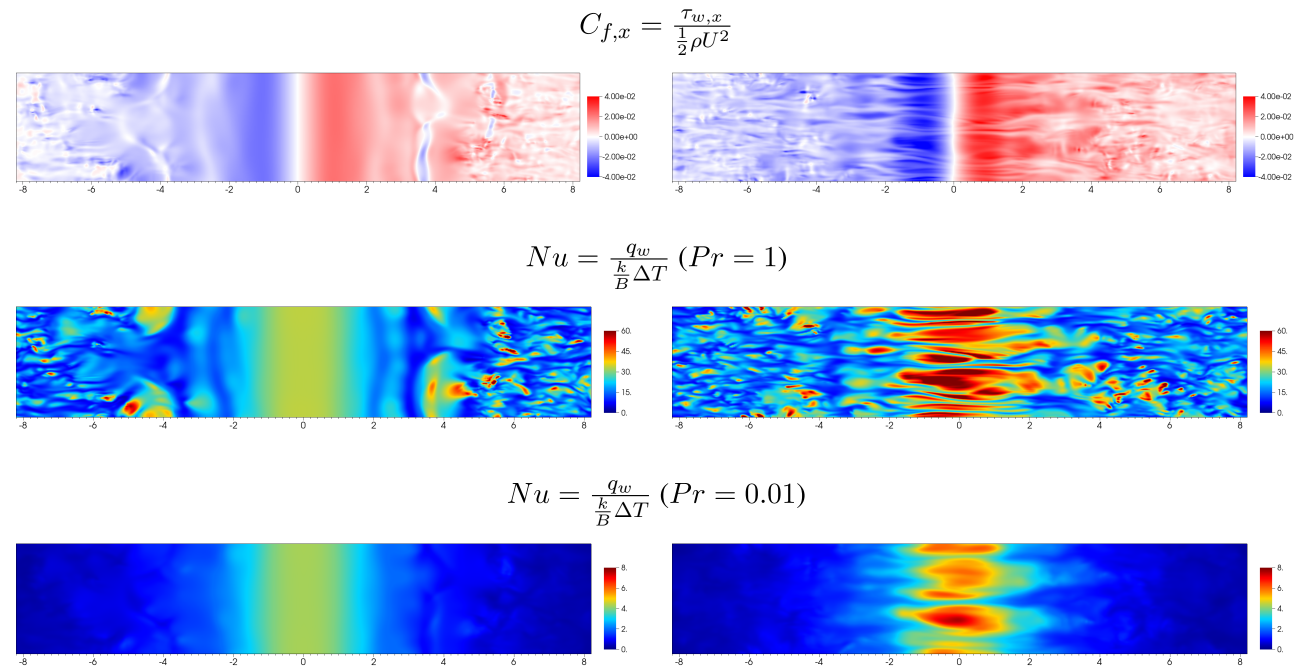

Figure 9. visualizations of the fluxes on the bottom wall. L4000 case (left), T4000 case (right), $Pr = 1$ (top), $Pr = 0.01$ (bottom).

streamwise streaks can be seen in both the wall shear-stress and the heat fluxes across the stagnation region for $|x|/B < 3$ in the turbulent case. These streaks are not present in the L4000 case where the stagnation line is also straight and unperturbed and where the boundary layers are laminar. In the L4000 case, however, strong spanwise structures can be observed, even leading to local recirculation around $x/B = 3.75$. They are maybe related to the Kelvin-Helmholz instability of the shear layer of the jet which produces strong spanwise vortices. In the L4000 case, the transition of the boundary layers occurs around $|x|/B = 5$, where small scale perturbations of wall-friction and heat flux are seen to appear. In the turbulent T4000 case, a transition occurs between $|x|/B = 3$ and $|x|/B = 4$ where the long streaks break down into shorter structures. Regarding the heat transfer, the elongated streamwise streaks significantly increase the heat transfer locally since the maximum local heat flux in the elongated streaks in T4000 is also twice higher than the laminar heat flux obtained in L4000 (Figure 9). As the Pr number is lowered, the Nu values are decreased and the turbulent fluctuations are smoothed. Yet, the elongated structures are still present for Pr as low as 0.01, but they are much wider than at $Pr = 1$. At $Pr = 0.01$, the Nu fluctuations in the turbulent region $|x|/B > 6$ are very small compared to the other cases where intense heat flux spots can still be observed for $|x|/B > 6$. Figure 10 compares (for the case T4000) the different AFM approaches for the turbulent heat flux modeling including results with the SGDH obtained by running the reference turbulence models on which those AFM were based: namely the Lien $k - \epsilon$ [34] and the Launder-Sharma $k - \epsilon$ [35] as detailed in [36]. In addition a non-isotropic turbulence model, but still based on the Reynolds analogy was also tested, the Reynolds Stress Model (RSM) using an elliptic blending (EB) [37] between a high Reynolds and low Reynolds models near walls. Results are presented for $Pr = 1$ (Figure 10 left) and $Pr = 0.01$ (Figure 10 right). At $Pr = 1$, and beyond the peak of the stagnation region, the DNS shows a plateau in the the Nusselt for $3 < x/B < 5$ which turns out to become a secondary maximum at $x/B \approx 6$ for the L4000 case as illustrated in [33]. For this T4000 case, the plateau corresponds to the zone where the streaks break as observed in Figure 9, while for the laminar case the secondary maximum corresponds at the

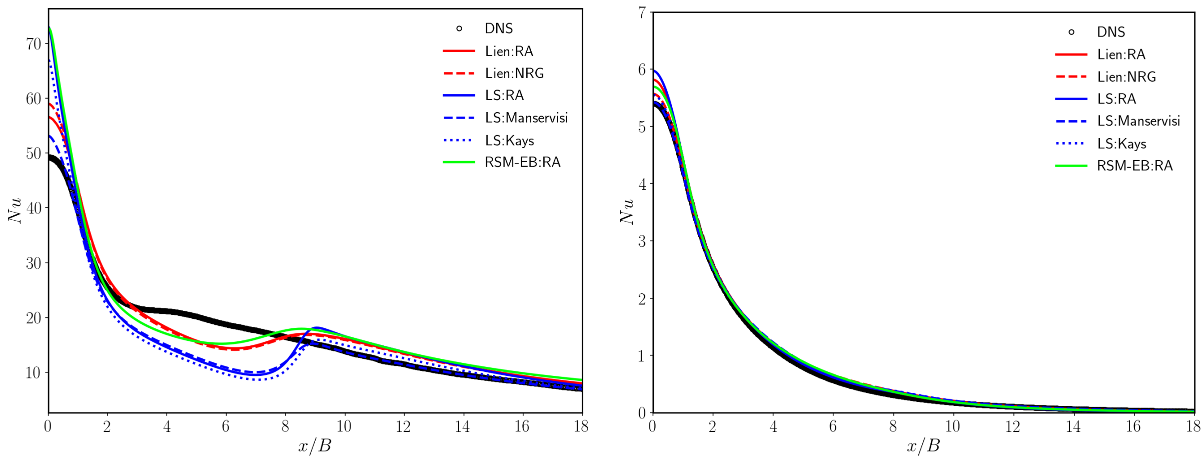

Figure 10. Nusselt Number for the T4000 case (from [36]). Left: $Pr = 1$. Right: $Pr = 0.01$.

laminar-turbulent transition of the wall boundary layer [33]. None of the tested RANS models is yet able to capture this plateau and their behavior looks closer to laminar than turbulent outside of the stagnation region. However, the $k-\epsilon-k_\theta-\epsilon_\theta$ of Manservisi and Meghini [20] performs better to capture the peak in the stagnation region as well $x/B > 9$. This region is where the boundary layer has fully transitioned and where the laminar and the turbulent profiles collapse (see [33]). At $Pr = 0.01$, the Nusselt has decreased and shows a more monotonic behavior. The explicit AFM [20] gives again the best performance even though both the AFM-NRG (Lien:NRG) and the classical SGDH model with the Kays correlation are very close.

Figure 11 and Figure 12 show the comparison of the different models for the temperature profile and the turbulent heat flux at the bottom wall respectively, for $Pr = 1$ and $Pr = 0.01$. At $Pr = 1$ the results are essentially driven by the turbulent momentum field as the Reynolds analogy is valid, hence the turbulence model used for momentum closure is mostly important here. For such cases, the RSM-EB model gives the best overall performance, even though the profile of the vertical turbulent heat flux is not well predicted by any of the model before transition (streaks break) occurs, e.g. $x/B < 5$. At Low Prandtl, models based on the Reynolds analogy are no more suited, and dedicated developed approaches offer the best results. Especially the $k-\epsilon-k_\theta-\epsilon_\theta$ (LS:Manservisi) is overall closer to DNS results followed by the AFM-NRG and the classical Launder-Sharma $k-\epsilon$ using the Kays correlation for the turbulent Prandtl number as advised in the previous section.

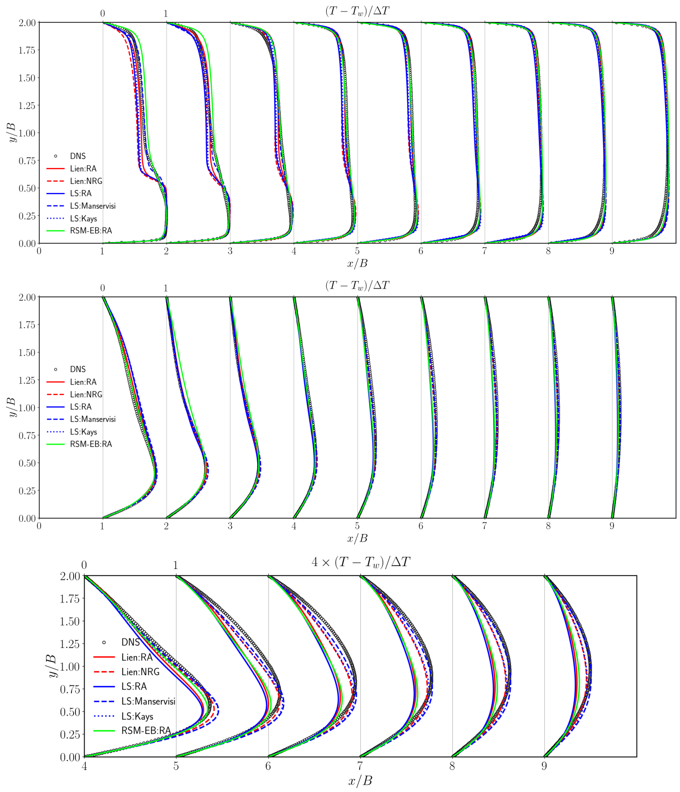

Figure 11. T4000 case. Vertical temperature profiles (from [36]). Top: $Pr = 1$. Middle: $Pr = 0.01$. Bottom: $Pr = 0.01$, temperature values multiplied by four to magnify differences.

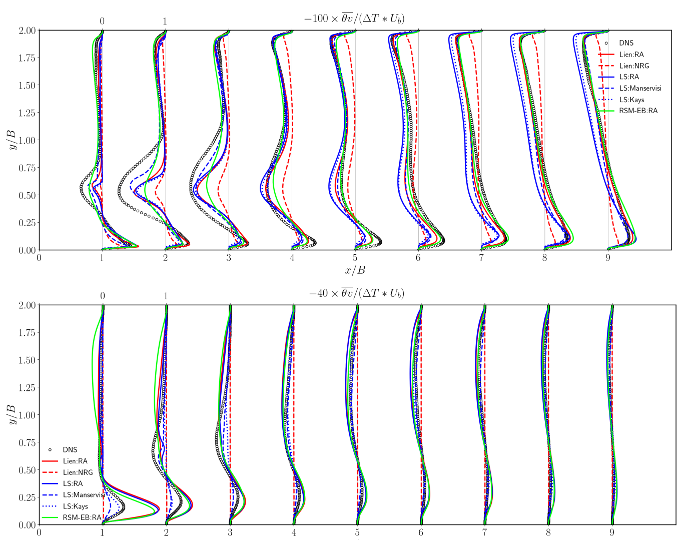

Figure 12. T4000 case. Vertical turbulent heat flux (from [36]). Top: $Pr = 1$. Bottom: $Pr = 0.01$ zoom.

3. CONCLUSION

This paper provided a brief overview on the relation between HiFi simulations and the assessment and development of dedicated approaches or best practice guidelines for RANS to compute turbulent forced convection in liquid metals. This work has been achieved through three EU funded projects, e.g. THINS, SESAME and MYRTE. For a sake of briefly, the paper only focused on some selected cases which were computed at UCLouvain. However, high fidelity simulations as well as RANS tests were performed on other cases as well as in other conditions such as mixed and natural convection. Nevertheless, the presented cases illustrated how HiFi simulations contributed to develop (i) new BPG guidelines if models based on the simple gradient diffusion hypothesis are used, and (ii) to develop and assess new approaches calibrated for low Prandtl number fluids such as the algebraic heat flux models. In the former case, a simple $k-\epsilon$ based model together with the Kays correlation for the turbulent Prandtl number and the mixed-wall-function is a good candidate for industrial simulations. In the latter case, AFM models (either implicit of explicit) could be a good choice in more complex situations such as mixed or natural convection or when strong turbulence anisotropy is expected (implicit AHFM-NRG). In this case, new approaches of these models based on the RSM-EB are emerging such as the AHFM-NRG-RSM-EB but still need to prove their performances. The main issue among those more advanced approaches is their lack of generality and their complexity in calibration of the increasing number of model constants. An interesting path that needs to be investigated would be the use of machine learning techniques to derive a general model of the turbulent heat flux components; this is being studied through a collaborative research between Von Karman Institute and UCLouvain.

ACKNOWLEDGMENTS

The work described in this paper has been funded by the Euratom research and training programmes under grant agreements No. 249337 (THINS, FP7) and No. 654935 (SESAME, H2020) . The present research benefited from computational resources made available on the Tier-1 supercomputer of the Fdration Wallonie- Bruxelles, infrastructure funded by the Walloon Region under the grant agreement No. 1117545. Computational resources have also been provided by the Consortium des Equipements de Calcul Intensif (CECI), funded by the Fonds de la Recherche Scientifique de Belgique (F.R.S.-FNRS) under Grant No. 2.5020.11 and by the Walloon Region.

REFERENCES

1. A. N. Kolmogorov, “The local structure of turbulence in incompressible viscous fluid for very large Reynolds number,” *Dokl. Akad. Nauk. SSR*, **30** (1941).

2. Y. Bartosiewicz and M. Duponcheel, “Large Eddy Simulation: application to liquid metal fluid flow and heat transfer,” in *Thermal Hydraulics Aspects of Liquid Metal Cooled Nuclear Reactors*, pp. 245 – 273, Elsevier, Woodhead Publishing, (2019).

3. Y. Bartosiewicz and M. Duponcheel, “Large Eddy Simulation: application to liquid metal fluid flow and heat transfer,” in *Thermohydraulics and Chemistry of Liquid Metal Cooled Reactors*, VKI Lecture Series, Von Karman Institute for Fluid Dynamics, (2017).

4. S. Corrsin, “On the spectrum of isotropic temperature fluctuations in an isotropic turbulence,” *Journal of Applied Physics*, **22** (1951).

5. G. Grötzbach, “Revisiting the resolution requirements for turbulence simulations in nuclear heat transfer,” *Nucl. Eng. Des.*, **241** (11), pp. 4379–4390 (2011).

6. R. Stieglitz and T. Schulenberg, "Flow measurement techniques in heavy liquid metals," *Nucl. Eng. Des.*, **240**, pp. 2077 – 2087 (2010).

7. A. Shams et al., "A Collaborative Effort Towards the Accurate Prediction of Turbulent Flow and Heat Transfer in Low-Prandtl Number Fluids," *Proc. The 18th International Topical Meeting on Nuclear Reactor Thermalhydraulics, NURETH-18*, (2019).

8. F. Roelofs et al., "Status and perspective of turbulence heat transfer modelling for the industrial application of liquid metal flows," *Nuclear Engineering and Design*, **290** (2015).

9. F. Roelofs, "Liquid Metal Thermal Hydraulics: State-of-the Art and Future Perspectives," *Proc. The 18th International Topical Meeting on Nuclear Reactor Thermalhydraulics, NURETH-18*, (2019).

10. O. Reynolds, "On the extent and action of the heating surface of steam boiler," *Proc. Proceedings of the Literary and Philosophical Society of Manchester*, (1874).

11. Y. Bartosiewicz, M. Duponcheel, M. Manconi, G. Winckelmans, and L. Bricteux, "Turbulence Modeling at Low Prandtl Number," in *Fluid Mechanics and Safety Issues in HLM Nuclear Reactors*, VKI Lecture Series, Von Karman Institute for Fluid Dynamics, (2013).

12. F. Roelofs, editor, *Thermal Hydraulics Aspects of Liquid Metal Cooled Nuclear Reactors* .

13. G. Grötzbach, "Challenges in low-Prandtl number heat transfer simulation and modelling," *Nuclear Engineering and Design*, **264** (0), pp. 41 – 55 (2013).

14. F. Dehoux, Y. Lecocq, S. Benhamadouche, R. Manceau, and L.-E. Brizzi, "Algebraic modelling of the turbulent heat fluxes using the elliptic blending approach - application to forced and mixed convection regimes," *Turbulence and Combustion*, **88** (1-2), pp. 77 – 100 (2012).

15. F. Dehoux, S. Benhamadouche, and R. Manceau, "An elliptic blending differential flux model for natural, mixed and forced convection," *International Journal of Heat and Fluid Flow*, **63**, pp. 190 – 204 (2012).

16. L. Bricteux, M. Duponcheel, G. Winckelmans, I. Tiselj, and Y. Bartosiewicz, "Direct and large eddy simulation of turbulent heat transfer at very low Prandtl number: Application to lead–bismuth flows," *Nucl. Eng. Des.*, **246**, pp. 91–97 (2012).

17. M. Duponcheel, L. Bricteux, M. Manconi, G. Winckelmans, and Y. Bartosiewicz, "Assessment of RANS and improved near-wall modeling for forced convection at low Prandtl numbers based on LES up to $Re_\tau = 2000$," *International Journal of Heat and Mass Transfer*, **75** (2), pp. 470 – 482 (2014).

18. A. Shams, F. Roelofs, E. Baglietto, S. Lardeau, and S. Kenjeres, "Assessment and calibration of an algebraic turbulent heat flux model for low-Prandtl fluids," *International Journal of Heat and Mass Transfer*, **79**, pp. 589 – 601 (2014).

19. A. Shams and A. D. Santis, "Towards the accurate prediction of the turbulent flow and heat transfer in low-Prandtl fluids," *International Journal of Heat and Mass Transfer*, **130**, pp. 290 – 303 (2019).

20. S. Manservisi and F. Menghini, "A CFD four parameter heat transfer turbulence model for engineering applications in heavy liquid metals," *Int. J. Heat Mass Tran.*, **69**, pp. 312–326 (2014).

21. S. Manservisi and F. Menghini, "Triangular rod bundle simulations of a CFD $k - \epsilon - k_\theta - \epsilon_\theta$ heat transfer turbulence model for heavy liquid metals," *Nuclear Engineering and Design*, **273**, pp. 251 – 270 (2014).

22. A. Shams et al., "Reference numerical database for turbulent flow and heat transfer in liquid metals," *Nucl. Eng. Des.*, **353**, pp. 110274 (2019).

23. O. Vasilyev, "High order finite difference schemes on non-uniform meshes with good conservation properties," *Journal of Computational Physics*, **157** (2), pp. 746–761 (2000).

24. L. Bricteux, M. Duponcheel, and G. Winckelmans, "A multiscale subgrid model for both free vortex flows and wall-bounded flows," *Phys. Fluids*, **21** (10), pp. 105102 (2009).

25. H. Kawamura, H. Abe, and Y. Matsuo, "DNS of turbulent heat transfer in channel flow with respect to Reynolds and Prandtl number effects," *International Journal of Heat and Fluid Flow*, **20** (3), pp. 196 – 207 (1999).

26. I. Tiselj, "DNS of turbulent channel flow at $Re_\tau = 395$, 590 and Pr=0.01," *Proc. The 14th International Topical Meeting on Nuclear Reactor Thermalhydraulics, NURETH-14*, (2011).

27. H. Abe, H. Kawamura, and Y. Matsuo, "Surface heat-flux fluctuations in a turbulent channel flow up to $Re_\tau = 1020$ with $Pr = 0.025$ and 0.71," *International Journal of Heat and Fluid Flow*, **25** (3), pp. 404 – 419 (2004).

28. L. Bricteux, M. Duponcheel, G. Winckelmans, and Y. Bartosiewicz, "DNS and LES of Turbulent Channel Flows at Very Low Prandtl Number: Application to convection in Lead-Bismuth," *Proc. The 14th International Topical Meeting on Nuclear Reactor Thermalhydraulics, NURETH-14*, (2011).

29. S. Hoyas and J. Jimenez, "Scaling of the velocity fluctuations in turbulent channels up to $Re_\tau = 2003$," *Physics of Fluids*, **18** (1), pp. 4 (2006).

30. W. Kays, "Turbulent Prandtl number - Where are we," *Journal of Heat Transfer-transaction Of The ASME*, **116** (2), pp. 284 – 295 (1994).

31. B. Kader, "Temperature and concentration profiles in fully turbulent boundary Layers," *Int. J. Heat Mass Tran.*, **24** (1451) (1981).

32. A. V. Ortiz, *Turbulent natural convection along a vertical plate for different Prandtl number fluids*, Phd thesis, Universit catholique de Louvain, Louvain-la-Neuve, Belgium, 2019.

33. M. Duponcheel and Y. Bartosiewicz, "Direct numerical simulations of low-Prandtl turbulent heat transfer in planar impinging jets," *Proc. The 18th International Topical Meeting on Nuclear Reactor Thermalhydraulics, NURETH-18*, (2019).

34. F. Lien, W. Chen, and M. Leschziner, "Low-Reynolds-Number Eddy-Viscosity Modelling Based on Non-Linear Stress-Strain/Vorticity Relations," in *Engineering Turbulence Modelling and Experiments*, edited by W. RODI and G. BERGELES, volume 3 of *Elsevier Series in Thermal and Fluid Sciences*, pp. 91 – 100, Elsevier, Oxford, (1996).

35. B. Launder and B. Sharma, "Application of the energy-dissipation model of turbulence to the calculation of flow near a spinning disc," *Letters in Heat and Mass Transfer*, **1** (2), pp. 131 – 137 (1974).

36. A. D. Santis, A. V. Ortiz, A. Shams, and L. Koloszar, "Modelling of a planar impinging jet at unity, moderate and low Prandtl number: Assessment of advanced RANS closures," *Annals of Nuclear Energy*, **129**, pp. 125 – 145 (2019).

37. R. Manceau and K. Hanjalic, "Elliptic blending model: A new near-wall Reynolds-stress turbulence closure," *Physics of Fluids*, **14** (2), pp. 744–754 (2002).